

Design of a 3 DOFs Parallel Actuated Mechanism for a Biped Hip Joint

R. Sellaouti, A. Konno, F. B. Ouedzou

Abstract— This paper deals with a novel approach to carry out the design of 3 DOF actuated joints for humanoid robots. Instead of common serial mechanism, a more robust parallel mechanism was developed. This kind of structure allows the terminal body to move within a cone from the nominal position and permits unlimited rotation about the cone pointing axis. Simulations were conducted to validate the kinematic model and optimize the design. Experimental prototype was developed to perform realistic tests on the control of this kind of mechanism.

Keywords— Parallel mechanism, Hip joint, Biped robot.

I. INTRODUCTION

It is generally admitted that one of the situations, where articulated locomotion is better than wheeled one, is involving in irregular terrains. Besides, considering that our private and professional environment is designed for humans, it becomes natural to admit humanoid robots as more adapted for such environment.

In fact humanoids open a large research background in many domains, like intervention in hostile areas, the design of human prostheses and familiar robots. Due to complicated techniques in the design and control of actuated legs, walking robots present many specific problems. The most important in such application is to insure static and dynamic stability with minimal energy consumption [1][2].

Many efforts have been produced by the scientific community since early 70's. Three decades of intense activity (especially in Japan and the United States) gave a large platform of walking machines [3][4], all different compared on their dynamic control and performances. Honda's humanoids P2 and P3 [5] and Waseda University's Wabian [6] are the representatives.

Such progress was possible thanks to essential works done all over the world. Raibert demonstrated in the late 80's that simple and decoupled techniques can control a walking biped [7]. Passive dynamics, which produce natural gaits and permits energetic economy, was studied by MacGeer [8].

The ROBIAN project (ANthropomorphic BIPed ROBot), is conducted in order to increase our under-

Authors are with the Laboratoire de Robotique de Paris 10, 12 Avenue de l'Europe, F 78140 Vélizy, France. E-mail: {sellaout,konno,ouezdou}@robot.uvsq.fr .

standing of the human being locomotion system and to develop a real testing bed for passive prosthesis [9]. This paper, presenting a novel design approach of 3 DOFs hip joints, deals with the project's design part.

Generally, the simplest way to design an actuated 3 DOFs joint is a serial design where the rotations are performed successively. The main advantage of such systems is the linearity of Input-Output relationships, which leads to an easier control. However, with the development of more performing control techniques we can use parallel mechanisms, which are more robust and more powerful for a given size.

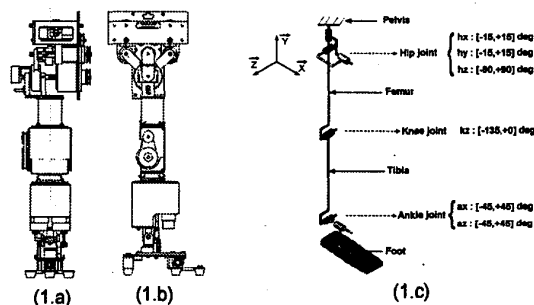


Fig. 1. ROBIAN's leg

The leg kinematic structure shown in Figure 1 is used in the ROBIAN project. The drawings (1.a) and (1.b) represent front and side views of the ROBIAN leg. The kinematic structure of this leg is shown on Figure (1.c). Joints angular position amplitudes given on this Figure are issued from biomechanics studies [13]. It is obvious that the three rotations in the human being hip have different ranges. Indeed the pitch rotation (around Z axis) has a range of 180 degrees. The roll (around Y axis) and yaw (around X axis) angles have a range which is six times less than the pitch range. Due to this difference between the hip joint angles ranges, non serial mechanism will be more convenient to reproduce the human hip joint motion during walk. Then, a novel mechanism, inspired from orientating platforms, is used for the actuated 3 dofs hip joint [10][11][12]. The parallel mechanism shown in Figure 2 allows the femur to move within a large range in one direction compared to the two others.

II. MECHANISM ARCHITECTURE

Figure 2 shows the mechanism architecture of the hip joint of ROBIAN. The mechanism is actuated by two linear actuators (LA1 and LA2) and a rotational one (RA). These actuators are attached to a fixed platform. Such configuration represents an interesting advantage compared to serial architecture because all actuators are fixed on the base (less moving mass). The two linear actuators LA1 and LA2 orientate a satellite platform via two intermediate axes (1) and (2). This orientation makes the movable body turn of q_2 and q_1 about Y and X axis respectively. So a conic area centered on his nominal position can be reached (Figure 2).

The final rotation q_3 , which have the largest range, is actuated by the rotational actuator. Then the total reachable positions will be given by rotating the cone about Z axis.

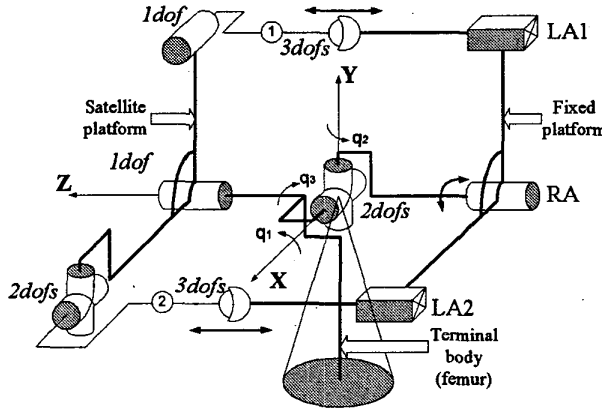


Fig. 2. Kinematics of ROBIAN hip joint

III. INVERSE KINEMATICS MODEL

To carry out the kinematic model of the chosen parallel actuated mechanism different coordinates systems are needed. These frames and the geometrical parameters of the structure are shown in Figure 3. Four coordinates systems are introduced as follows:

- $\mathcal{R}_b = (O, X_b, Y_b, Z_b)$: fixed coordinates system,
- $\mathcal{R}_t = (O_1, X_t, Y_t, Z_t)$: terminal coordinates system,
- $\mathcal{R}_i = (O_1, X_i, Y_i, Z_i)$: intermediate coordinates system attached to satellite platform,
- $\mathcal{R}_{pt} = (O_1, X_{pt}, Y_{pt}, Z_{pt})$: preterminal coordinates system obtained from \mathcal{R}_b with two successive rotations around fixed axis, q_2 about Y_b and q_1 about X_b .

With such a parameterization, the frames \mathcal{R}_t and \mathcal{R}_i are obtained from \mathcal{R}_{pt} by a rotation respectively of q_3 and β around Z_{pt} . The transformation matrix between \mathcal{R}_b and \mathcal{R}_i can be obtained as follows:

$$\begin{pmatrix} X_i \\ Y_i \\ Z_i \end{pmatrix} = T \cdot \begin{pmatrix} X_b \\ Y_b \\ Z_b \end{pmatrix} \quad (1)$$

where,

$$T = \begin{pmatrix} C_2 C_\beta + S_1 S_2 S_\beta & C_1 S_\beta & S_1 C_2 S_\beta - S_2 C_\beta \\ S_1 S_2 C_\beta - C_2 S_\beta & C_1 C_\beta & S_1 C_2 C_\beta + S_2 S_\beta \\ C_1 S_2 & -S_1 & C_1 C_2 \end{pmatrix}$$

and,

$$\begin{aligned} S_i &= \sin(q_i) \\ C_i &= \cos(q_i) \quad i = 1, 2 \\ S_\beta &= \sin(\beta) \\ C_\beta &= \cos(\beta). \end{aligned}$$

The mechanism fixed parameters are the following :

- $OA = OB = O_2 A_2 = O_2 B_2 = a$
- $B_1 B_2 = A_1 A_2 = d$
- $O_1 O_2 = l$
- $OO_2 = h$
- $\widehat{BOA} = \widehat{B_2 O_2 A_2} = 90^\circ$

The three actuator outputs values are:

- $AA_1 = h_1$ for LA1,
- $BB_1 = h_2$ for LA2,
- α for RA.

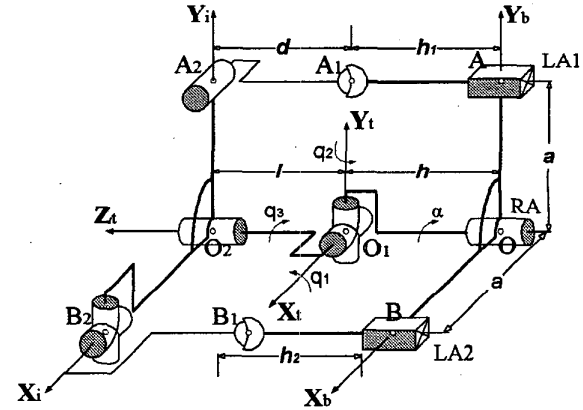


Fig. 3. Kinematic structure

A. Inverse kinematics solutions

The inverse kinematics model consists of determining h_1 , h_2 and α as functions of q_1 , q_2 and q_3 . To solve this model, at first we will try to extract h_1 , h_2 and β for given q_1 and q_2 , and then, α will be determined in a straight manner from input-output relationship of a universal joint.

The geometrical constraints of the structure are represented by the following three equations :

$$\|\overrightarrow{B_1 B_2}\| = d \quad (2)$$

$$\|\overrightarrow{A_1 A_2}\| = d \quad (3)$$

$$\overrightarrow{A_1 A_2} \cdot \mathbf{X}_i = 0 \quad (4)$$

The constraint given by equation (4) is due to the fact that the joint axis on A_2 is always perpendicular to $\overrightarrow{A_1 A_2}$ (see Figure 3).

Developing these constraints, three scalar equations depending on varying parameters ($q_1, q_2, h_1, h_2, \beta$) and fixed parameters (a, b, l, h) are obtained:

$$(h - h_2)^2 + (h - h_2)(2lC_1C_2 - 2aS_2C_\beta + 2aS_1C_2S_\beta) + l^2 - d^2 + 2a^2(1 - C_2C_\beta - S_1S_2S_\beta) - 2alC_1S_2 = 0 \quad (5)$$

$$(h - h_1)^2 + (h - h_1)(2lC_1C_2 + 2aS_2S_\beta + 2aS_1C_2C_\beta) + l^2 - d^2 + 2alS_1 + 2a^2(1 - C_1C_\beta) = 0 \quad (6)$$

$$(h - h_1)(-S_2C_\beta + S_1C_2S_\beta) - aC_1S_\beta = 0 \quad (7)$$

Before solving the system, a simple case is isolated: It is easily derived from equation 7 that if \mathbf{X}_i is perpendicular to \mathbf{Z}_b i.e. $S_2C_\beta = S_1C_2S_\beta$, then $S_\beta = 0$. In this case h_1 and h_2 are easily determined by the equations (5) and (6).

Eliminating this case, $(h - h_1)$ is obtained from (7). Replacing this expression in (6) the following equation is given:

$$A_1C_\beta + A_2S_\beta + A_3S_\beta C_\beta + A_4S_\beta^2 + A_5C_\beta^2 = 0 \quad (8)$$

Where,

$$\begin{aligned} A_1 &= -2a^2C_1S_2^2 \\ A_2 &= 2a^2S_1C_1S_2C_2 \\ A_3 &= -2(l^2 - d^2)S_1S_2C_2 - 2al(S_1^2S_2C_2 + S_2C_2) - 4a^2S_1S_2C_2 \\ A_4 &= (l^2 - d^2)S_1^2C_2^2 + 2alS_1C_2^2 + a^2C_1^2 + 2a^2S_1^2C_2^2 \\ A_5 &= (l^2 - d^2)S_2^2 + 2alS_1S_2^2 + 2a^2S_2^2 \end{aligned}$$

Replacing S_β by $2X_\beta/(1 + X_\beta^2)$ and C_β by $(1 - X_\beta^2)/(1 + X_\beta^2)$ where $X_\beta = \tan(\beta/2)$, the following fourth order polynomial is obtained:

$$a_4X_\beta^4 + a_3X_\beta^3 + a_2X_\beta^2 + a_1X_\beta + a_0 = 0 \quad (9)$$

Where,

$$\begin{aligned} a_4 &= -A_1 + A_5 \\ a_3 &= 2A_2 - 2A_3 \\ a_2 &= 4A_4 - 2A_5 \\ a_1 &= 2A_2 + 2A_3 \\ a_0 &= A_1 + A_5 \end{aligned}$$

The resolution of this equation gives β . Known β , the two parameters h_1 and h_2 are calculated from (5) et (7) respectively.

Finally the last parameter α is directly obtained from Input-Output relationship of universal joint as:

$$\alpha = \arctan \left[\frac{C_2 \tan q_3}{C_1 + S_1S_2 \tan q_3} \right] \quad (10)$$

B. Numerical analysis

A program was developed using C++ language to solve numerically the inverse kinematics. The Laguer's resolution method was used to find the solutions of the fourth order equation (9) [14]. An additional work was necessary to be integrated in this study. It consists of numerical detection of singular regions. In fact the mechanism can involve in four mathematically possible configurations. These configurations shown in Figure 4 are separated by singular positions defined geometrically as follows:

$$\overrightarrow{A_1 A_2} \perp \mathbf{Z}_i \quad (11)$$

$$\overrightarrow{B_1 B_2} \perp \mathbf{Z}_i \quad (12)$$

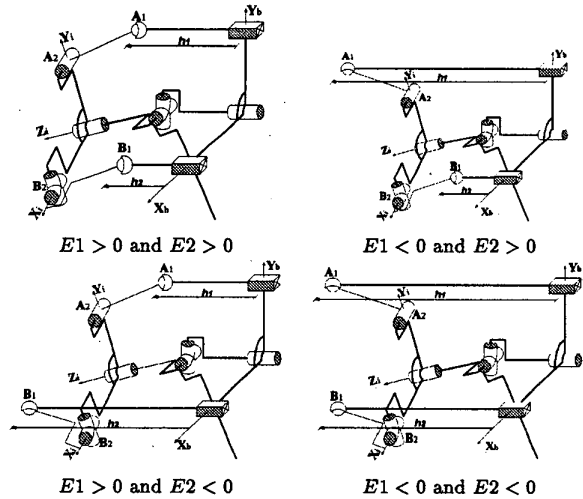


Fig. 4. Four possible kinematic configurations

In fact, the simplest way to mathematically define these configurations is to study the sign of the scalar products:

$$\begin{aligned} E1 &= \text{sign}[\overrightarrow{A_1 A_2} \cdot \mathbf{Z}_i] \\ &= \text{sign}[(h - h_1)C_1C_2 + l + aS_1] \quad (13) \end{aligned}$$

$$\begin{aligned} E2 &= \text{sign}[\overrightarrow{B_1 B_2} \cdot \mathbf{Z}_i] \\ &= \text{sign}[(h - h_2)C_1C_2 + l - aC_1S_2] \quad (14) \end{aligned}$$

A combination of these binary conditions gives the four configurations. Nevertheless, due to the rigidity and simplicity of the first configuration, only the case where E1 and E2 are positive was studied. The figure (5), shows the working domain for a mechanism with the following parameters values: $a=0.09$ m, $d=0.03$ m, $l=0.01$ m and $h=0.050$ m.

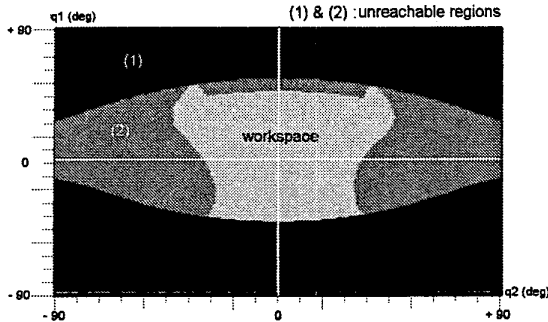


Fig. 5. Workspace of the parallel mechanism

Studying the variation of the working domain, preponderant parameters were found. In fact, the ratios $\rho_1 = \frac{d}{a}$ and $\rho_2 = \frac{l}{d}$ give the global shape of the domain. For the hip joint, the criteria chosen to find the parameters of the structure was the symmetry of the working region. As shown in the shots of the Figure 6, a couple of ratios ($\rho_1 = \frac{1}{3}, \rho_2 = \frac{1}{3}$) gives an adequate structure.

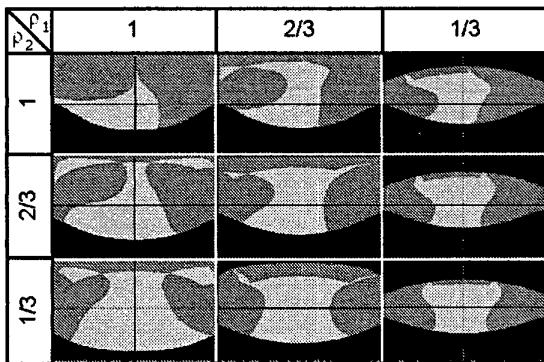


Fig. 6. Working domains Vs. parameters (ρ_1, ρ_2).

IV. SIMULATIONS

Simulations on the software ADAMS¹ were proceeded to validate the numerical analysis (Figure 7). Two main interpretations submerged from this work. The first one is the importance of parameter a on

¹Product of Mechanical Dynamics Inc, www.ADAMS.com

the system characteristics. In fact, the forces required from linear actuators deeply depend upon this parameter. So optimization were needed to fix its value.

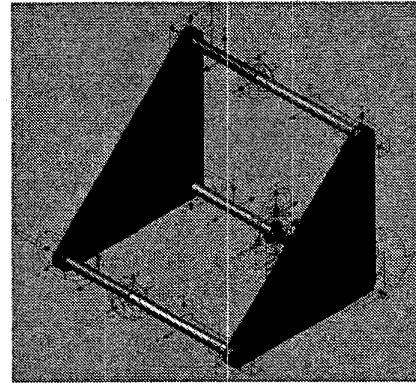


Fig. 7. Simulation model

On the other hand, optimization of the mechanism orientation about Z axis was proceeded. In fact, for the hip joint application a kinematic simulation demonstrated that a rotation about 45 degrees of the structure represent the best configuration to have a distributed cooperation between the linear actuators for walking task (comparable power consumption). The simulation model was animated with biomechanics data for the roll and yaw motions (see Figure 8).

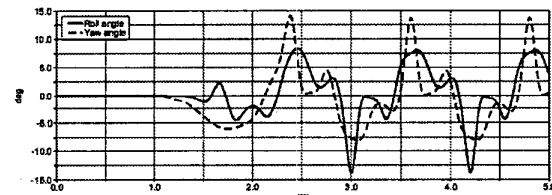


Fig. 8. Roll and Yaw

The first kinematic results are for a basic configuration where the structure's coordinates system \mathcal{R}_b have the same axis as the hip's coordinates system \mathcal{R} (see Appendix: Figure 13). In the second, the structure is rotated with an angle of 45 degrees around the Z axis (see Appendix: Figure 14).

This configuration introduces changes on the inverse kinematics program. So to tally the mechanism with it's given application, a correspondence between angles (q_1, q_2, q_3) of the parallel structure and (Yaw: h_x , Roll: h_y , Pitch: h_z) of the hip joint was integrated. The Figure 9 shows the transformation of the workspace after this rotation.

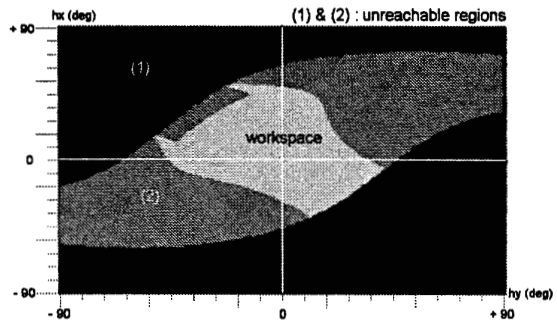


Fig. 9. Workspace after 45 deg rotation

V. EXPERIMENTS

In order to validate manufacturing possibilities and find the design critical devices, a test platform was developed. The overview of the experimental setup is shown in Figure 10. The system is composed of:

- The parallel structure actuated by three DC motors,
- Motor drivers¹,
- BIA's micro controllers²,
- Control interface.

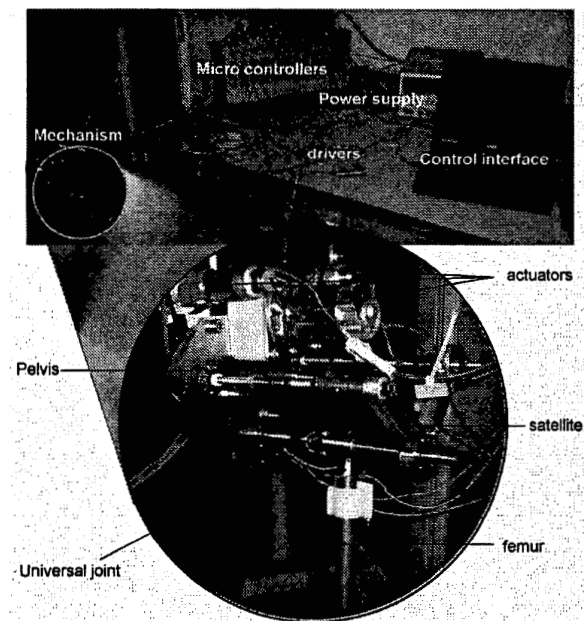


Fig. 10. Experimental setup

Many experimentations are conducted on this platform. A low level one, consists of the initialization

¹Okazaki Sangyo Co, www.okatech.com

²BIA France, www.bia.fr

of the mechanism using the nonlinearity of the Input-Output relationships. In fact iterative basic tests, consisting of the comparison of the outputs of the mechanism and the inverse kinematics solution for given input, allows accurate detection of the nominal position. The higher level experimentation, consist of preparing a control architecture for such systems. In this context, it was demonstrated that encoding the angle β gives a powerful feedback for the control.

VI. DESIGN

ROBIAN biped weights 25 kilograms. Owing to the lack of forces information on the hip, approximations of torques were introduced. Pessimist configurations of the biped robot gave the needed actuating power. For the yaw and roll dofs a combination of 20 watt DC motors and ball screw transformation was used. And for pitch dof a combination of 90 watt DC motor and harmonic drive was chosen. Figure 11 shows the final design of the hip joint.

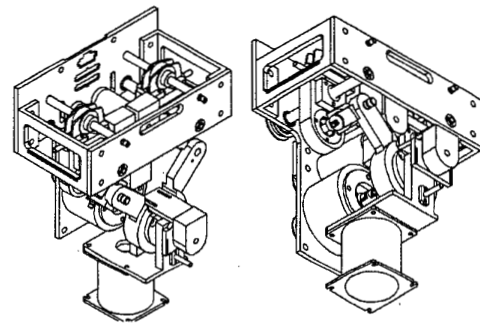


Fig. 11. ROBIAN hip joint

VII. CONCLUSION

Rigidity and power consumption are two critical points on humanoid design. In this paper a novel 3dofs parallel mechanism for ROBIAN hip joint was presented. Two main advantages justify the choice of such structure for this anthropomorphic biped robot. The first advantage is the rigidity of its parallel structure compared to a serial one for the same size. The second one is the power consumption economy given by cooperation between actuators during the walk and especially less mass in movement.

After the presentation of the parallel structure, the inverse kinematics was studied. A program was developed to solve the inverse kinematics model. Numerical analysis were conducted to optimize the structure and validate the inverse kinematics. A dynamic simulation was performed to analyze the mechanisms power consumption and introduce its real application. Finally,

an experimental platform was developed with standard components to improve the simulation results and perform control tasks.

A similar 2dofs ankle mechanism is developed. This actuated ankle joint is inspired from the hip joint structure by eliminated the central dof (q_3). A prototype of ROBIAN biped robot is being developed with a novel hip and ankle parallel joints (see Figure 12).

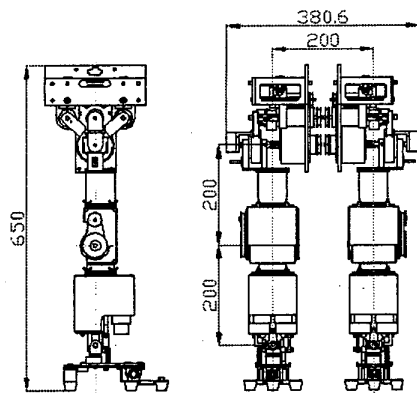


Fig. 12. ROBIAN's lower limb design

REFERENCES

- [1] Jong H. Park, Yong K. Rhee, "ZMP Trajectory Generation for Reduced Trunk Motions of Biped Robots," *Inter. Conf. on Intelligent Robots and Systems*, Proceedings of the IEEE, 1998.
- [2] David W. Robinson, Jerry E. Pratt, Daniel J. Paluska and Gill A. Pratt, "Series Elastic Actuator Development for Biomimetic Walking Robot," *Inter. Conf. on Adv. Intelligent Mechatronics*, Proceedings of the IEEE, 1999.
- [3] M. Gienger, K. Löffler and F. Pfeiffer, "A Biped Robot that Jogs," *Inter. Conf. on Robotics and Automation*, Proceedings of the IEEE, April 2000.
- [4] Bernard Espiau, *BIP: A Joint Project for the Development of an Anthropomorphic Biped Robot*, the BIP team, INRIA Rhône-Alpes, 1997.
- [5] K. Hirai, M. Hirose, Y. Haikawa and T. Takenaka, "The development of honda humanoid robot," *Inter. Conf. on Robotics and Automation*, Proceedings of the IEEE, May 1998.
- [6] J. Yamaguchi, S. Inoue, D. Nishino and A. Takanishi, "Development of a Bipedal Humanoid Robot Having Antagonist Driven Joints and Three DOF Trunk," *Inter. Conf. on Intelligent Robots and Systems*, Proceedings of the IEEE, 1998.
- [7] Marc H. Raibert, *Legged robots that balance*, MIT Press, Cambridge, MA, 1986.
- [8] Tad MacGeer, "Passive Dynamic Walking," *International Journal of Robotics Research*, Vol.9, No.2, pp.62-82, 1990.
- [9] F. Gravez, O. Bruneau and F.B. Ouedzou, "Three-Dimensional Simulation of Walk of Anthropomorphic Biped," *ROMANSY*, 2000.
- [10] J. P. Merlet, "Trajectory verification in the workspace for parallel manipulators," *The Int. J. of Robotics research*, 13(4), pp.326-333, August 1994.
- [11] J.A. Carretero, M. Nahon and R.P. Podhorodeski, "Workspace analysis of a 3-dof parallel mechanism," *Inter. Conf. on Intelligent Robots and Systems*, Proceedings of the IEEE, 1998.

- [12] S.K. Agrawal, Glen Desmier and Siyan Li, "Fabrication and Analysis of a Novel 3 DOF Parallel Wrist Mechanism," *Journal of Applied Mechanics*, Vol.117, pp.343-345, 1995.
- [13] David A. Winter, "Biomechanics of human movement," *Wiley-interscience publication*, 2nd Edition, New York, 1990.
- [14] W.H. Press, S.A. Teukolsky, W.T. Vetterling and B.P. Flannery, "Numerical Recipes in C," *Cambridge University Press*, Second Edition, pp.371-374, 1992.

APPENDIX

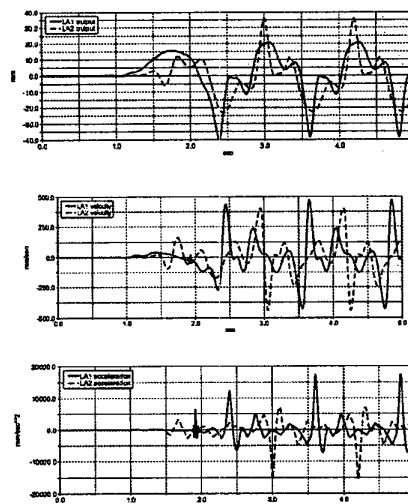


Fig. 13. Simulation results for basic orientated structure

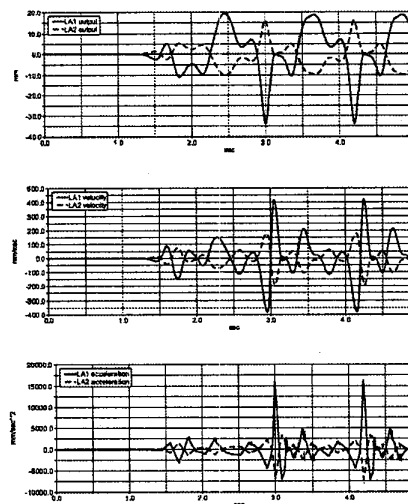


Fig. 14. Simulation results for rotated structure